Computers and Electronics in Agriculture 104 (2014) 1–8

Contents lists available at ScienceDirect

Computers and Electronics in Agriculture

journal homepage: www.elsevier.com/locate/compag

Automatic detection of powdery mildew on grapevine leaves by image analysis: Optimal view-angle range to increase the sensitivity

Roberto Oberti [a,*], Massimo Marchi [a,b], Paolo Tirelli [a,b], Aldo Calcante [a], Marcello Iriti [a], Alberto N. Borghese [b]

[a] Department of Agricultural and Environmental Sciences-DISAA, Università degli Studi di Milano, via Celoria 2, Milano 20133, Italy
[b] Applied Intelligent Systems–AIS Lab, Computer Science Department, Università degli Studi di Milano, via Celoria 26, Milano 20133, Italy

ARTICLE INFO

Article history:
Received 5 November 2013
Received in revised form 20 February 2014
Accepted 4 March 2014

Keywords:
Disease detection
Grapevine
Powdery mildew
Multispectral imaging
Proximal sensing
Precision pest management

ABSTRACT

Powdery mildew is a major fungal disease for grapevine (*Vitis vinifera* L.) as well as for other important specialty crops, causing severe damage, including yield loss and depreciation of wine or produce quality. This disease is thoroughly controlled by uniform spraying of vineyards with agrochemicals according to a calendar, which can easily result in ten to fifteen fungicide applications in several grapevine-growing areas. Since primary infections are localized in discrete foci rather than being uniformly diffused, there are potential benefits linked to the development of systems able to detect initial infection foci and operate targeted treatments instead of the current homogenous and unselective sprayings.

Proximal optical sensing is a major candidate for becoming the preferred technique for identification of foci for powdery mildew in grapevine and other specialty crops, but detection sensitivity of symptoms in the early-middle stage can yield largely limited results due to the combination of small dimensions, low density, and spatial arrangement of thin fungal structures.

This study investigated how the detection sensitivity (i.e., the portion of diseased tissue correctly recognized by the system) can be improved, especially for early-middle symptoms by means of sensing measurements carried out from an angle, rather than perpendicularly to the leaf's surface. To this aim, a multispectral imaging approach was applied to 35 grapevine leaves (10 used as calibration and 25 as validation samples) that were imaged at five different view angles from 0° (camera perpendicular to the leaf surface) up to 75°. Detection sensitivity was evaluated by applying to the validation images an algorithm based on the combination of two spectral indexes. The used algorithm was separately trained basing on the calibration set of images.

Overall results indicate that detection sensitivity generally increases as the view angle is increased, with a peak value obtained for images acquired at 60°. In particular, for tissue with early-middle symptoms, the algorithm's sensitivity exhibits a dramatic improvement, from 9% at 0° up to 73% at 60°.

Provided that the adopted training system results in rather homogenous leaves orientation, these findings suggest that field-sensing systems for detecting initial foci of grapevine powdery mildew can achieve improved results by providing the capability of measuring the canopy from a view angle in the range of 40–60°.

1. Introduction

In current viticulture practice, fungicides are applied uniformly through the vineyard according a spraying calendar, rarely triggered by experts' decisions and weather conditions, but more typically based on regular and frequent fungicide application. For powdery mildew, a major grapevine (*Vitis vinifera* L.) disease caused by the fungus *Erysiphe necator* Schwein (syn. *Uncinula necator* Schwein); this continuous protection approach can easily result in carrying out up to ten or even more treatments per season, in many vineyards of some of the most important wine-producing regions worldwide (Stummer et al., 2003; Calonnec et al., 2004; Crisp et al., 2006a,b; Iriti et al., 2011).

The polycyclic ascomycete *E. necator* is recognized worldwide as a major disease affecting both grape yield and quality. Susceptibility to powdery mildew depends on cultivar and environmental factors. Warm conditions with high relative humidity are favoring the development of the disease. In spring, primary infections can arise very early from overwintering mycelium in the buds, giving rise to the so-called "flag-shoot" or from ascospores overwintering in plant debris, which are then disseminated in the vineyard.

* Corresponding author. Tel.: +39 0250316867.
E-mail address: roberto.oberti@unimi.it (R. Oberti).

http://dx.doi.org/10.1016/j.compag.2014.03.001
0168-1699/

Secondary infections are propagated by conidia differentiated in conidiophores, eventually evolving in disease patches that in turn produce fresh inoculum for following infection epidemics.

The pathogen colonizes the epidermal tissues of green organs (leaves, shoots, and bunches), causing severe damage to vineyards, including yield loss and depreciation of wine quality. Currently, in the warmer and drier grapevine-growing areas, powdery mildew is thoroughly controlled by agrochemicals, including contact, local, and systemic fungicides sprayed uniformly in vineyards (Stummer et al., 2003; Calonnec et al., 2004; Crisp et al., 2006a,b; Iriti et al., 2011).

Despite this spatially homogenous control approach, primary infection sites are characterized by a localized, discrete distribution rather than being uniformly diffused. Indeed, flag shoots and overwintering ascospores are randomly disseminated throughout the vineyard with an initially very low spatial density.

From this, it can be argued that chemical control of powdery mildew in grapevine would greatly benefit from a system able to target the protection treatments on the primary infection foci in a timely fashion. Indeed, especially during the early stages of disease development, detection of initial symptoms and their selective and targeted treatment would prevent the establishment of the infection and its epidemic spread to wider patches or to whole vineyard. This approach is currently being explored within the EU-funded project CROPS (www.crops-robots.eu).

Among possible solutions for automatic disease symptom detection, proximal optical sensing has specific characteristics particularly relevant in the view of field applications on grapevine and other fruit-tree crops (Oberti, 2003): (i) it performs non-destructive measurements, allowing for repeated acquisitions during the season without interfering with crop growth; (ii) it does not require direct contact with the sample, so it can be operated from almost any desired proximal distance; (iii) it is based on practically instantaneous phenomena, compatible with on-the-go measurements from a vehicle at normal field-operation speed; and (iv) it can inspect the vertical structure of the canopy, with a potential detection capability of early disease symptoms at a centimeter or even sub-centimeter scale.

Sensor technologies for crop diseases have been extensively reviewed by Sankaran et al. (2010) recently, while a more focused discussion on applications of proximal optical sensing for disease detection both in arable and specialty crops can be found in West et al. (2003) and Lee et al. (2010), respectively.

Moshou et al. (2011) developed a tractor-mounted, multi-sensor prototype integrating hyperspectral and multispectral images through real-time data-fusion techniques, demonstrating field functionality in automatic disease detection on wheat, enlarging the site-specific spraying research framework to include autonomous robotic platforms actuation.

However, the research dedicated to proximal optical detection of grapevine diseases is still limited to a few studies. Naidu et al. (2009) investigated the potential of using the leaf reflectance changes induced by grapevine leafroll-associated virus (GLRaV-3) as a diagnostic tool by measuring the VIS–NIR–MIR spectra of detached leaves. They found that the most discriminant wavelength intervals between healthy and virus-infected leaves are in the spectral region of green (near 550 nm), near infrared (near 900 nm), and in mid-infrared (near 1600 nm and 2200 nm). Calcante et al. (2012) evaluated experimentally the capability of two commercial optical devices (GreenSeeker RT100TM, Crop Circle TM) in discriminating different levels of downy mildew (*Plasmopara viticola*) infection on detached grapevine leaves, finding a fairly linear relationship between the disease severity and the processed output data from the tested sensors. Poutaraud et al. (2007) used in vivo fluorescence measurements on leaves inoculated with downy mildew (*P. viticola*) to study the spatial distribution of grapevine stilbenic phytoalexins (protectant secondary metabolites synthetized under stress conditions). They found that the high-intensity blue-violet fluorescence (F390 nm) emitted by stilbenes allowed to detect the stilbenes' local accumulation on the abaxial side of leaves, leading the authors to conclude that stilbenes fluorescence of leaves can be a promising early marker of pathogens attacks. With reference to powdery mildew, Bélanger et al. (2008) also applied fluorescence measurements to detect and quantify infection symptoms on detached grapevine leaves. By investigating different emission/excitation wavelength combinations, finding that the ratio between blue (F440 nm) and green (F520 nm) fluorescence intensity of healthy and diseased areas of leaves showed significantly different results starting from three days after inoculation.

Fungal diseases typically affect leaf reflectance, and for powdery mildew this is particularly due to the proliferation of hyphae filaments of the mycelium on the hosting tissue, leading gradually to a whitish-gray, powdery appearance. Nevertheless, at early-middle stages of mycelium development, these thin filamentous structures are barely detectable since the combination of their small dimensions, low density, and spatial arrangement has low influence on the spectral signature of the leaf surface, which in turn limits the detectability of the disease by optical sensing systems based on reflectance measurements.

During preliminary field measurements on grapevine, however, we have noticed that, thanks to the light back-scattered by hyphae and conidia whitish filaments, the detection of powdery mildew symptoms at early stages can be evidently improved when looking at leaf surface from an angle instead of looking perpendicularly to it. Interestingly enough, when studying proximal optical detection of winter wheat's fungal diseases (including powdery mildew) Zhang et al. (2012) and Yuan et al. (2013) underlined the necessity of investigating the influence of leaf orientations in disease detection by spectral reflectance.

Since in grapevine and other specialty crops, tractor-mounted optical sensing systems are typically used to scout the vegetation from the front of the canopy (i.e., mostly looking perpendicular to leaves faces), in the present study we investigate how the view angle can affect the detection's sensitivity of powdery mildew in grapevine leaves. This study is conducted by applying a multispectral imaging approach based on a relatively simple algorithm designed to this aim and hereafter described. The obtained results are expected to provide valuable information on possible optimization of the configuration of a field system for automatic detection of powdery mildew in grapevine and other specialty crops prone to this disease.

2. Material and methods

2.1. Plant material

Plants of *V. vinifera* L. cv Cabernet Sauvignon were propagated from wood one-bud cuttings, grown in 25 cm diameter pots filled with a mixture of sand and loamy soil (3:1, v/v). They were maintained in a greenhouse under controlled conditions at 25/20 °C day/night temperature, with 75% relative humidity and a 16-h photoperiod (40 μmol quanta m^{-2} s^{-1}). Plants were regularly watered and fertilized (Na/P/K/Mg, 15:10:15:2) and no pesticide treatment was applied. At the age of four months, 25 plants with approx. 15–20 leaves each were selected from the batch and were used in the experiment due to their healthy status of vegetation, as ascertained by visual inspections by plant pathologists. Seven plants were kept isolated under controlled conditions in order to maintain healthy conditions, while 18 plants were separately inoculated with the aim of obtaining a wide range of symptoms.

2.2. Fungal isolates and inoculation

The isolates of *E. necator* used in this study originated from infected fresh leaf material (*V. vinifera* cv Groppello) collected in an experimental vineyard. Grapevines were inoculated by brushing conidia from freshly sporulating colonies onto the adaxial (upper face) epidermis of healthy leaves in order to establish different disease foci on each plant. The inoculum density (conidia per cm^2) used in each experiment was determined by placing glass microscope slides at arbitrary locations inside the vegetation during inoculation, and by counting the number of conidia in 10 views at 50× magnification by a light microscope (Olympus BX 50, Tokyo, Japan). The used inoculum density ranged approximately from 60 to 500 (mean 248) conidia per cm^2, depending on the experiment.

2.3. Angular imaging setup

In vivo images of single grapevine undetached leaves under varying viewing angles were acquired by using a rotating table holder contained in a 0.8 m × 0.8 m × 1.5 m box acting as darkroom; a standing frame equipped with a multi-spectral camera; and a set of diffuse illumination light sources (Fig. 1).

The multi-spectral camera (MS4100, RedLake, USA) had three different CCDs acquiring images in three spectral channels: green (center wavelength at 540 nm), red (660 nm), and near infrared (800 nm). Image resolution was 1912 × 1076 pixels with 8 bit for each channel. Each sample leaf (Fig. 1-a) of a measured plant (Fig. 1-b) was vertically held by a position-adjustable dark background panel (Fig. 1-c). This allowed to adequately flatten the leaf surface, as well as to facilitate the foreground automatic recognition in image processing. The plane (Fig. 1-d) holding the plant sample could be rotated around the vertical axis by a defined angle, thus permitting the acquisition of leaf surface images from different view angles by the multi-spectral camera (Fig. 1-e), which was instead maintained in a stationary position together with the diffuse illumination sources (Fig. 1-e). For each measured leaf, the vertical position of the camera on the stand-frame was adjusted so that the distance and relative orientation between leaf and camera was kept constant for all the measurements. Stable, diffuse, and reproducible sample illumination was obtained by artificial light with a set of halogen lamps and white panel reflectors which projected indirect diffuse light on the imaged leaf. Unwanted ambient light was removed by enclosing the measurement setup in the darkroom box that had an open front side from which images were taken and diffuse illumination was provided.

The camera was placed at a distance of 0.5 m from the leaf sample, resulting in an image spatial resolution of about 0.15 mm/pixel. Gain and integration time of the camera were manually set and kept constant for all the acquisitions. The repeatability of measurements conditions was checked by keeping in the field of view of the camera three reflectance standard panels (Spectralon $R = 0.20$, $R = 0.50$ and $R = 0.99$; Labsphere, USA) and by monitoring their average gray-level intensity during the acquisition.

2.4. Measurement procedure

Four, 8, and 16 days after inoculation, the infected plants were visually inspected to evaluate symptoms appearance. At each inspection date, leaves exhibiting specific symptoms were selected and labeled. The sample leaves were chosen so that a complete and representative range of disease symptoms was obtained at the end of the whole experiment. In parallel, among healthy plants, healthy leaves of different ages were also selected and labeled.

Prior to images acquisition, all labeled leaves were visually inspected by a plant pathologist and classified according to disease symptoms presence and intensity (see Section 2.5).

By using the measurement setup described above, in vivo images of undetached labeled leaves were acquired from five different view angles changed at steps of 20°, namely 0°, 20°, 40°, 60°, and 75°. The largest considered angle was limited to 75°, since beyond this limit the visible portion of the leaf's surface was too much reduced by the extreme viewing geometry.

During the three dates, 35 different leaf samples were measured, obtaining a total of 175 images (5 angles per leaf), covering a range of leaf ages (young to mature), powdery mildew intensity (healthy to necrotic tissues), and possible interfering pigmentations.

2.5. Reference disease assessment

Prior to images acquisition, each selected and labeled leaf underwent a pathological survey, and the position, dimensions, and intensity of fungal symptoms were accurately recorded on a paper-printed picture of the leaf sample. All significant features other than powdery mildew symptoms, such as local chlorosis or pigmentations related to nutritional or physiological disorders other than disease, were also recorded as possible source of false positives for automatic disease detection algorithm.

Fig. 1. Measurement setup for in vivo leaf imaging at different view angles: (a) imaged leaf; (b) sample plant; (c) adjustable background; (d) rotating holding plane; (e) multispectral camera; (f) diffuse illumination sources.

In particular, the powdery mildew symptomatic regions on each selected leaf were scored for disease by a plant pathologist according to a 0–4 arbitrary infection-level scale, as follows:

- IL = 0 (infection level 0), corresponding to small (1–2 mm in diameter) chlorotic spots likely expected to develop fungal mycelium.
- IL = 1, small areas (1–2 mm) with hyphae at the initial stage of development (rare and hard to see with the naked eye).
- IL = 2, areas (2–8 mm) with middle stage mycelial structures (both hyphae and conidiophores visible with careful observation).
- IL = 3, extended colonies (8–20 mm) with evident gray-whitish powdery appearance.
- IL = 4, brown senescent–necrotic lesions.

2.6. Calibration and validation sets of images

The measured leaves and their corresponding images were divided into two separate sets: calibration (10 leaf samples) and validation (25 leaf samples).

Within the calibration images, areas among all those classified (healthy, symptomatic with different infection levels, pigmentations other than disease) by the reference survey of the pathologist, were randomly selected. Inside each selected area, ROIs (region of interest) of 10 × 10 pixels each were manually extracted. Since the actual size of the leaf sector considered was typically larger than the sampled ROIs, it was generally possible to keep the 10 × 10 ROIs within the leaf sectors at all view angles despite their smaller area due to the projection. At 75° due to the extreme projection, in a number of cases the sampled ROI had smaller pixels size, to be kept within the considered leaf sector.

The total number of ROIs extracted from the calibration images for the different classes were chosen to obtain a distribution among healthy tissue (20 ROIs), powdery-mildew-infected tissue (30 ROIs, with a balanced distribution among different disease stages), and necrotic (7 ROIs) and other pigmented tissue (7 ROIs).

Each ROI selected on a specific leaf image was repeatedly extracted by hand in the corresponding images acquired at the other view angles. Particular care was taken so that the five repeated ROIs in the five images acquired at different view angles were corresponding to the same sector of leaf tissue.

The selected ROIs from the calibration set were subsequently used to tune the disease detection algorithm and to train the classification parameters (Section 3.2).

To evaluate the algorithm's results obtained on the validation set of images, the areas identified as disease by the reference survey were carefully "transcribed" onto a digital copy of each acquired images. Operatively, any symptomatic area detected on a leaf by the pathological survey was manually drawn as a colored mask onto a copy of the digital images acquired for that specific leaf, carefully keeping the position and the dimensions recorded by the expert. For different infection levels, different hue codes were used when drawing the colored masks (Fig. 2).

The validation set of images was subsequently used to test the automatic disease detection algorithm, and the obtained results were evaluated by comparison with the colored masks (i.e. by applying a logical AND combination of algorithm outputs and colored masks).

3. Disease detection algorithm

A multi-spectral image analysis algorithm for automatic detection of powdery mildew disease was designed, validated, and applied to test if the sensitivity of symptoms identification can be improved by proper view angle of the leaf. The functional details of the algorithm are as follows.

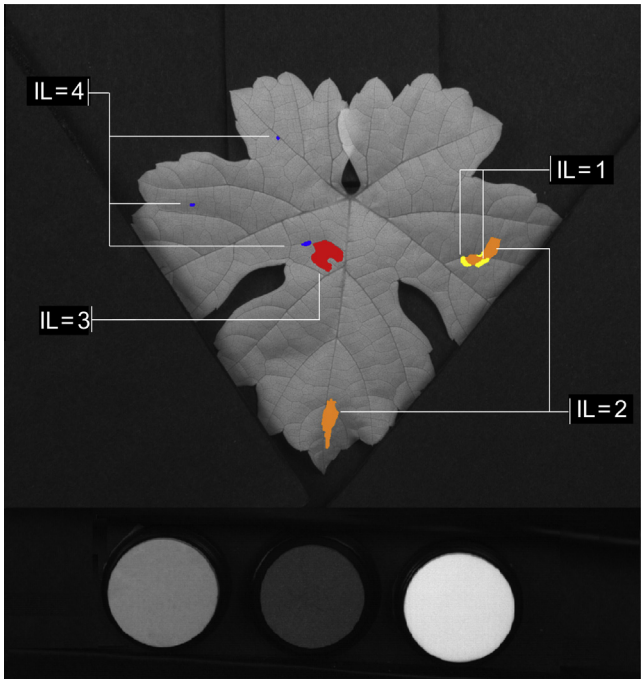

Fig. 2. Example of validation image acquired at 0° view angle. The colored masks were manually drawn according to in vivo pathological survey of the leaf. The shown masks were subsequently used as reference pixels classification to assess the disease detection algorithm results. Unpainted pixels on the leaf surface correspond to healthy tissue; yellow masks correspond to early infection (IL = 1, see Section 2.5 for infection level scale); in orange middle symptoms (IL = 2); in red advanced symptoms (IL = 3); in blue small spots of necrotic tissue (IL = 4). Labels are just shown for illustrative purposes. The shown leaf sample does not exhibit any symptom in previsual stage (IL = 0). (For interpretation of the references to colour in this figure legend, the reader is referred to the web version of this article.)

3.1. Foreground discrimination

The first step is the separation of the leaf tissue from the background. The use of a dark background panel in the images acquisition setup allowed to obtain a bimodal distribution of pixel intensities in the near-infrared channel, with low gray levels for the background and high levels for leaf tissue. This enabled an accurate foreground segmentation by fitting a Gaussian mixture to the histogram of NIR pixels intensities by implementation of an Expectation Maximization algorithm (Bishop, 2006).

3.2. Healthy/diseased tissue classifier

A preliminary analysis of the pixels intensity distribution in the red, green, and near-infrared channels was conducted on the ROIs of the calibration set, previously defined in Section 2.6. The distribution of raw values of gray levels in the three channels did not allow a clear discrimination between healthy and diseased areas. Nevertheless, this discrimination can be largely enhanced by using appropriate spectral indices, i.e., algebraic combinations of pixel's gray levels in two or more spectral channels (Oberti, 2003; Devadas et al., 2009; Rumpf et al., 2010; Mahlein et al., 2012).

The following two spectral indices were used in this study:

$$I1 = (\mathrm{Red} * \mathrm{Green})/\mathrm{NIR}\hat{}2 \quad (1)$$

$$I2 = \mathrm{Red}/(\mathrm{Red} + \mathrm{Green} + \mathrm{NIR}) \quad (2)$$

The index I1 is designed to respond to reflectance variations in either red or green channel, i.e., to respond to expected major changes in tissue color. Indeed, any local change (increase) of gray level in one of these two channels contributes to changing the value of the numerator of I1, while the denominator acts as a normalization term for any local change in the illumination level, being the NIR intensity unaffected by disease symptoms presence, unless at very advanced stages. The index I2 represents the red component on the total intensity of the pixel. Given that the red channel overlaps the chlorophyll absorption band, the numerator of I2 is expected to be low for healthy tissue (due high absorption by chlorophyll), while to become significantly higher in presence of powdery mildew hyphae. The denominator in I2 acts again as a normalization term for illumination.

In summary, the spectral indexes I1 and I2 are expected to give significantly lower values for healthy pixels compared to those obtained for pixels in diseased areas.

Fig. 3 shows how healthy and disease pixels from the training set are mapped in the plane defined by indexes I1 and I2, for images acquired at different view angles. As expected, the data from healthy tissue are grouped in low values range for both I1 and I2, while the data from diseased tissue appear more sparsely distributed. Indeed, pixels corresponding to initial up to advanced disease symptoms (IL = 1–3) are shifted toward higher ranges of I1 and I2, resulting in only partial overlap with healthy pixels. Moreover, pixels from senescent–necrotic areas (IL = 4) are clearly separated in an upper region of the plane.

Quite remarkably, it is apparent from this figure that while the position of the cluster of healthy data (approx. $I1 \leqslant 0.2$ and $I2 \leqslant 0.17$) remains unchanged as the view angle varies, the distribution of disease pixels (IL = 1–3) gradually shifts and expands towards high values of I1 and I2 as the view angle increases. As a result, in the plane (I1, I2), the separation among healthy and diseased pixels increases noticeably with the angle, likely making powdery mildew symptoms (IL = 1–3) more and more detectable by increasing the view angle of the leaf.

Due to the plume-shaped distribution of healthy data in the (I1, I2) plane, a quadratic function (parabola) was chosen as the boundary to separate the region corresponding to healthy pixels from that corresponding to disease symptoms pixels. To determine the specific equation's parameters of the parabolic boundary, the data of the training set were used by applying the following conditions:

(i) The axis of the parabola was rotated to be parallel to the first eigenvector of the covariance matrix of the healthy values, i.e., it was chosen to be coincident with the major axis of healthy data distribution.
(ii) The parabola was set to intersect the line oriented as the second eigenvector of the covariance matrix (i.e., the minor axis of the healthy data distribution) and passing through the healthy centroid; the distance of the two intersection points from the centroid was arbitrarily equaled to 5 standard deviations of the data distribution along the minor axis (i.e., 5 times the square root of the second eigenvalue of healthy values).
(iii) Finally, the position of the parabola's vertex was iteratively determined by gradually shifting the vertex coordinates along the axis from the healthy centroid towards the disease pixel group; the shift iterations were stopped when the position reached by the parabola resulted to separate the healthy and disease calibration group so that the number of diseased pixels misclassified as healthy (i.e., false negatives left out from the disease decision region) equaled 2 times (an arbitrary, yet rational, threshold) the number of healthy pixels misclassified as diseased (i.e., false positives erroneously included in the disease decision region).

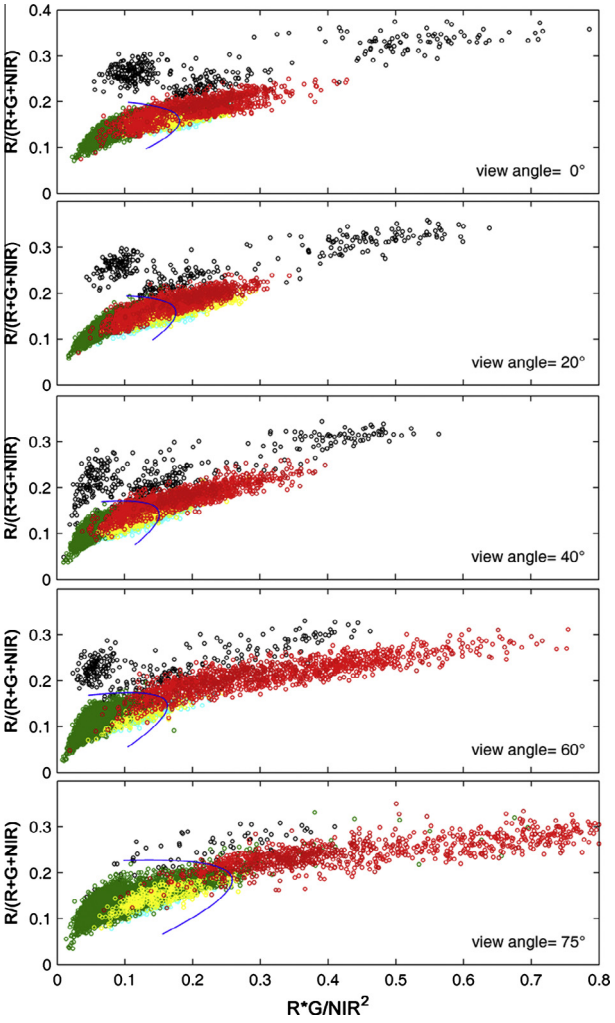

Fig. 3. Distribution of values of indexes I1 and I2 (see Eqs. (1) and (2) in the text) computed for pixels in ROIs of the training set belonging to different classes: green = healthy tissue; red = initial to advanced powdery mildew symptoms (infection level IL = 1–3, see Section 2.3); black = senescent–necrotic tissue (IL = 4); yellow = pre-symptomatic areas (IL = 0). From top to bottom: distribution of the data obtained for images acquired at a view angle of 0°, 20°, 40°, 60° and 75°, respectively. In each sub-graph the blue solid line represents the quadratic discriminating function separating the decision regions corresponding to healthy and disease tissue for each view angle. (For interpretation of the references to colour in this figure legend, the reader is referred to the web version of this article.)

In Fig. 3, the resulting parabolas computed from the training data collected at each of the five view angles considered in this study are plotted as blue solid lines in the corresponding sub-graphs.

For each considered view angle, the sub-regions of the plane determined by the corresponding parabolic boundary were subsequently used as decision regions for automatic classification of pixels in acquired images.

3.3. Algorithm implementation and test on validation set

The computation of spectral indexes and a corresponding classification based on the decision regions in the plane (I1, I2) was implemented into a disease detection algorithm. After background removal (see Section 3.1), for each foreground pixel, the pair value of indexes I1 and I2 are computed by applying Eqs. (1) and (2). If the computed pair falls inside the healthy decision region defined as described above (see Section 3.3), then the pixel is classified as

healthy tissue; otherwise, it is classified as potentially diseased tissue.

After these steps, a set of binary regions is obtained identifying the tissue areas likely to correspond to disease symptoms (if any). However, as a result of measurement noise, sparse small areas or single isolated pixels can also be included within the identified binary regions. Noise pixels are filtered out by applying a 3×3 binary opening.

The binary regions left after morphological filtering are finally assumed to correspond to diseased areas, while the rest of the image foreground is assumed to correspond to healthy leaf tissue.

The described algorithm was applied to the validation set of images in order to test its capability to automatically discriminate healthy and diseased tissue areas. To this aim, the algorithm output was compared with the reference results of the pathological survey, coded as colored masks in reference images.

4. Results and discussion

The disease detection algorithm was applied to the images of validation sets acquired at different view angles. As an illustrative example, Fig. 4 shows the results obtained with automatic detection of powdery mildew on the validation sample previously represented in Fig. 2. This leaf is of particular interest since it exhibits on its surface symptoms of different levels: it has small areas at initial stage of disease development on the right side (IL = 1, yellow areas in Fig. 4a), surrounded by a wider patch at a more advanced stage (IL = 2) as another area in the lower part (orange areas in Fig. 4a). A region with more extended symptoms (IL = 3) is also present in the middle of the surface (red area in Fig. 4a), with few small necrotic lesions (IL = 3, blue areas in Fig. 4a) in the left upper side.

Using as a reference this classification obtained from the phyto-pathological survey, Fig. 4b–f shows the results obtained by the detection algorithm on the images of this leaf sample acquired at view angle 0°, 20°, 40°, 60°, and 75° respectively. In Fig. 4b–f, the unpainted area corresponds to healthy tissue correctly classified by the algorithm (true negatives), green areas correspond to diseased tissue at any infection level correctly recognized as disease (true positives), brown areas correspond to diseased tissue misclassified as healthy (false negatives), and orange areas correspond to healthy tissue misclassified as diseased (false positives).

Fig. 4b and c (view angles of 0° and 20°) show that the algorithm only detected the symptoms at advanced stages of infection (IL = 3 and IL = 4). This is indicated by the green masks (corresponding to true positive detections) in the middle and upper left part of the leaf face. On the other hand, the symptoms in the lower and right side (IL = 1 and IL = 2) remained mostly undetected, as indicated by the wide brown masks corresponding to false negative detections.

At larger view angles of 40° and 60° (Fig. 4c and d), the detection of symptoms in advanced stage resulted even better, as indicated by the incremented area covered by green masks in the middle and upper left part of the leaf, where regions at IL = 3 and IL = 4 are present.

Interestingly, at these view angles also symptoms at early-middle stages of infection (IL = 1 and IL = 2) were detected by the algorithm as shown by wide green masks presence also in the lower and right side of the leaf surface. At angle 75° (Fig. 4f), leaf image results occluded by the extreme view geometry; nevertheless, symptoms detection capability for diseased areas present in the image appears confirmed.

False positives (orange masks in Fig. 4b–f) resulted to be mostly limited to small areas on veins, leaf/background border, or regions contiguous to detected symptoms.

These results are generally confirmed for the whole validation set, as shown by Table 1. This summarizes the overall automatic detection results obtained at different view angles and subdivided for each infection level assigned by phyto-pathological survey.

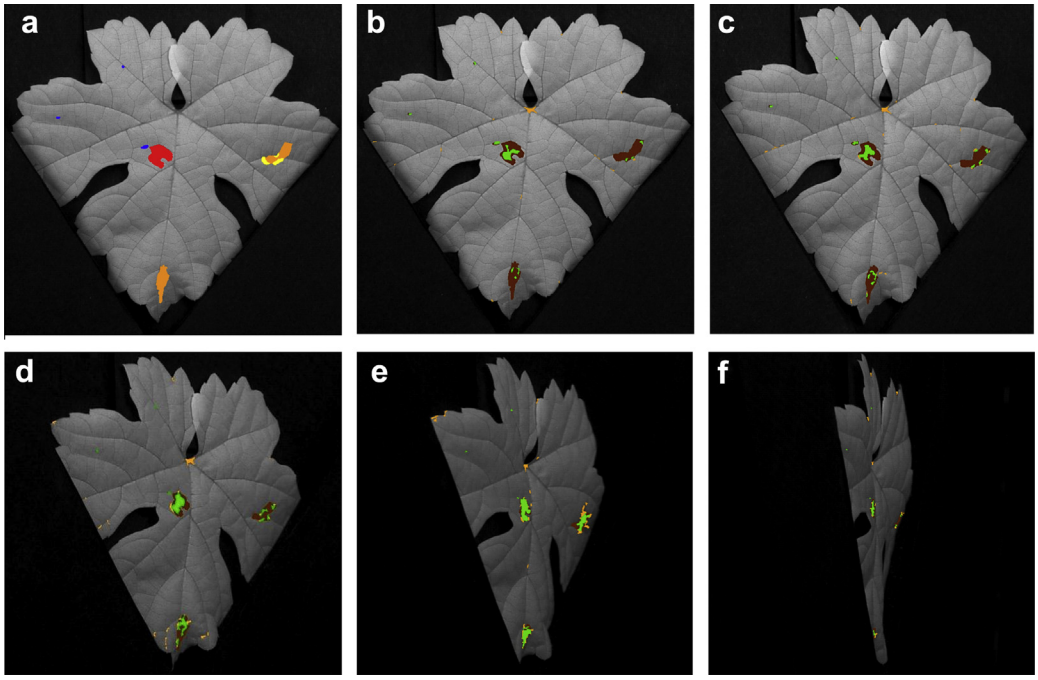

Fig. 4. Example of automatic detection of powdery mildew obtained by applying the algorithm to images of a validation leaf viewed from different angles. Results of automatic detection are compared with symptoms detected by a plant pathologist. (a) Ground truth, manual identification of symptoms on the leaf surface and their classification according to infection stage level by phytopathological survey (see Fig. 2 for color masks description). (b–f) Algorithm classification of leaf tissue with view angle at 0°, 20°, 40°, 60°, and 75° respectively; unpainted area corresponds to healthy tissue correctly classified (true negatives); green areas correspond to diseased tissue correctly classified (true positives); brown areas correspond to diseased tissue misclassified as healthy (false negatives); orange areas correspond to healthy tissue misclassified as diseased (false positives). (For interpretation of the references to colour in this figure legend, the reader is referred to the web version of this article.)

Table 1
Main results of automatic classification obtained by applying the disease detection algorithm to the validation set images acquired at the five view angle considered in the study.

View angle (°)	Analyzed pixels (manually classified)		Algorithm classification overall statistics		Sensitivity on diseased areas at different levels of infection				
	Disease	Healthy	NPV (%)	Sensitivity (%)	IL = 0 (%)	IL = 1 (%)	IL = 2 (%)	IL = 3 (%)	IL = 4 (%)
0	184,567	15,058,727	99.3	41.3	6.0	6.3	8.6	61.3	83.2
20	159,514	14,009,486	99.1	48.9	2.3	14.9	14.5	73.3	82.6
40	127,348	10,903,172	98.8	56.2	4.8	22.1	28.0	81.8	91.7
60	70,579	6,149,750	99.4	72.1	12.2	32.3	72.8	97.2	85.4
75	26,186	2,553,034	99.3	57.9	2.8	8.1	42.9	86.6	89.5

While the number of leaf samples is the same for each view angle, the total number of pixels analyzed by the algorithm decreases as the angle varies from 0° to 75°, obviously due to the reduction of the portion of leaf surface viewed by the camera. The percentage of pixels manually classified as disease resulted to be rather independent from the angle, ranging around 1.5% of the total foreground tissue. This unbalanced composition of the datasets (approx. 99/1 healthy to diseased ratio) reflects what is likely to be found in real field conditions, when searching for disease at early enough stage of development, i.e., searching spatially localized and discrete foci.

The total negative predictive value (NPV) obtained with the automatic classification, i.e., the fraction of pixels correctly recognized as not diseased (healthy) by the algorithm, resulted almost above 99% for all view angles. This means that for the all validation sets of images, about 99% of the pixels classified as healthy by the algorithm actually corresponded to real healthy tissue, according to the phyto-pathological survey. The minimum portion of disease pixels misclassified as healthy was obtained with the validation images acquired at 60°, for which the NPV value was slightly higher than others view angles.

A major indicator of the overall classification capability of an algorithm is its sensitivity, defined as:

$$\text{Sensitivity} = \text{TP}/(\text{TP} + \text{FN}) \quad (3)$$

and expressing the fraction of true positives (TP) outcomes on the total actual positives (true positives and false negatives) as defined by the reference method. In our specific case, the detection sensitivity (3) measures the fraction of the tissue manually classified as diseased that the algorithm correctly recognized as disease.

Table 1 indicates that the overall algorithm's sensitivity improves as the view angle is increased, reaching a peak value of 72% for validation images acquired at an angle of 60°. These results quantitatively confirm that powdery mildew symptoms become more and more detectable by increasing the view angle of the leaf (within a practical limit to avoid the occlusion to visibility of a too-large portion of leaf surface).

The last columns of Table 1 highlight also interesting patterns of algorithm's sensitivity for different disease infection levels. Indeed, by restricting the analysis to areas manually classified as IL = 0, corresponding to very early, pre-symptomatic disease stages, the algorithm's sensitivity had a very limited result, with a maximum value of only 12% obtained at 60°. On the other hand, when tissue classified at more advanced infection levels is considered, the algorithm's sensitivity exhibits a coherent improvement as the view angle is increased from 0° to 60°,while at 75° this relationship is less evident, being the leaf visibility partially occluded by the extreme viewing geometry. Indeed, for disease areas at IL = 1 the algorithm sensitivity resulted in a gradual increase from 6% up to 32% as the view angle was increased.

Noticeably, at IL = 2 when symptoms correspond to more developed fungal structures, the increment of sensitivity found at larger view angles is dramatic, passing from 9% at 0° to 73% at 60°. At IL = 3, with view angle of 60° the algorithm correctly recognized almost all the pixels that were manually classified as disease, resulting in a sensitivity of 97.2%. Anyway, at this stage of infection the automatic detection was quite efficient also at lower angles (e.g., the sensitivity at 0° was 61%). Similarly, pixels from senescent–necrotic areas (IL = 4) were effectively classified by the algorithm with a sensitivity well above 80% regardless the view angle.

These results confirm that at more advanced stages of infection (IL = 3 and IL = 4), disease symptoms can be optically detected from any view angle. Less obviously, the findings of this work indicate that at early-middle stages of infection (IL = 1 and IL = 2), powdery mildew symptoms are poorly detectable when sensed from angles perpendicular to the leaf surface; but if measurements are carried out from wide enough view angles, the sensitivity of the detection can be dramatically increased, even for quite early symptoms.

The reason for this may likely be related to the fact that at initial stages the filamentous structures of the mycelium start to grow vertically from hosting tissue, and hence their impact on leaf reflectance can be largely emphasized by observing by an angle the back-scattered light from these structures. After a certain stage of development, the mycelium layers accumulate on the leaf tissue, giving a whitish-gray, powdery appearance, detectable from any view angle.

These results have practical implications when considering instrumental field monitoring of powdery mildew on grapevine and on other specialty crops prone to this disease. Indeed, considering that in trellised vine-crops leaves mostly tend to be bended toward the inter-row space, a proximal-sensing optical system operated to frontally scout the vegetation can take advantage by viewing the canopy from an angle. But since around this average geometry, leaves in canopy exhibit a natural variability in orientation, it seems more appropriate to define an optimal range of view angles, rather than a specific value (which can be optimal for a leaf but not for those having slight different orientation).

This study suggests that detectability of powdery mildew can be significantly improved by adopting an appropriate measurement setup, which should include sensors geometry allowing canopy viewing by an angle in the range of about 40–60°. Even if obtained under illumination conditions designed to simulate natural diffuse light, these quantitative findings strongly rely on controlled orientation of leaf's faces allowed by laboratory conditions. Their extrapolation to field conditions should be limited to crops training system which result in rather homogenous orientation in foliage, and still has to be confirmed by suitable experiments.

5. Conclusions

This study investigated how the detection's sensitivity (i.e., the fraction of diseased tissue correctly recognized by the system) of powdery mildew on infected grapevine leaves may be improved by adopting appropriate view angles.

To this aim, a multispectral imaging approach based on a relatively simple disease detection algorithm was applied to a dataset of grapevine leaf samples exhibiting symptoms at different levels. The results obtained by automatic analysis of images at five view angles, from 0° to 75°, indicate that:

- The overall algorithm's sensitivity generally improves as the view angle is increased, reaching a peak value for images acquired at 60°, with 72% of pixels belonging to diseased tissue (regardless to the specific infection level of the symptoms) correctly detected by the algorithm.
- For symptoms at more advanced stage of development (corresponding to infection levels IL = 3 and IL = 4 according to the scale adopted in the study), the algorithm's detection sensitivity resulted fairly high for all the view angles, with values between 61% and 97%.
- For tissue with symptoms at early-middle infection levels, the algorithm's sensitivity exhibits a coherent improvement as the view angle is increased from 0° to 60°; in particular, at IL = 2 with fungal structures at the initial stage of development and visible with an accurate survey, the increment of sensitivity for automatic detection was dramatic, passing from 9% at 0° up to 73% at 60°.
- For regions exhibiting very early, pre-symptomatic disease stages (IL = 0) the algorithm's sensitivity resulted very limited, with a maximum value of only 12% obtained at 60°.
- Results obtained at a view angle of 75° tend to deviate from the above patterns, being the leaf visibility significantly occluded by the extreme viewing geometry

These results have practical implications for the development of a system for automatic detection of powdery mildew on grapevine (and other specialty crops) by proximal optical sensing. Indeed, provided that the plants training system results in rather homogenous leaves orientation, this study suggests that detectability of the disease at early-middle stages might be significantly improved by providing the setup with the capability of measuring the canopy by a view angle in the range of 40–60°.

Acknowledgments

This study was conducted within the project CROPS.

CROPS (GA-246252) is funded by the European Commission under the 7th Framework Programme within the theme "Automation and robotics for sustainable crop and forestry management".

References

Bélanger, M.C., Roger, J.M., Cartolaro, P., Viau, A.A., Bellon-Maurel, V., 2008. Detection of powdery mildew in grapevine using remotely sensed UV-induced fluorescence. Int. J. Remote Sens. 29, 1707–1724.

Bishop, C.M., 2006. Pattern Recognition and Machine Learning. Springer Science + Business Media, New York.

Calcante, A., Mena, A., Mazzetto, F., 2012. Evaluation of "ground sensing" optical sensors for diagnosis of *Plasmopara viticola* on vines. Spanish J. Agric. Res. 10, 619–630.

Calonnec, A., Cartolaro, P., Poupot, C., Dubourdieu, D., Darriet, P., 2004. Effects of *Uncinula necator* on the yield and quality of grapes (*Vitis vinifera*) and wine. Plant Pathol. 53, 434–445.

Crisp, P., Wicks, T.J., Bruer, D., Scott, E.S., 2006a. An evaluation of biological and abiotic controls for grapevine powdery mildew. 2. Vineyard trials. Aust. J. Grape Wine Res. 12, 203–211.

Crisp, P., Wicks, T.J., Lorimer, M., Scott, E.S., 2006b. An evaluation of biological and abiotic controls for grapevine powdery mildew. 1. Greenhouse studies. Aust. J. Grape Wine Res. 12, 192–202.

Devadas, R., Lamb, D.W., Simpfendorfer, S., Backhouse, D., 2009. Evaluating ten spectral vegetation indices for identifying rust infection in individual wheat leaves. Precision Agric. 10, 459–470.

Iriti, M., Vitalini, S., Di Tommaso, G., Di Tommaso, D., Faoro, F., 2011. A new chitosan formulation induces grapevine resistance against powdery mildew and improves grape quality traits. Aust. J. Grape Wine Res. 17, 263–269.

Lee, W.S., Alchanatis, V., Yang, C., Hirafuji, M., Moshou, D., Li, C., 2010. Sensing technologies for precision specialty crop production. Comput. Electron. Agric. 74, 2–33.

Mahlein, A.K., Oerke, E.C., Steiner, U., Dehne, H.W., 2012. Recent advances in sensing plant diseases for precision crop protection. Eur. J. Plant Pathol. 133, 197–209.

Moshou, D., Bravo, C., Oberti, R., West, J.S., Ramon, H., Vougioukas, S., Bochtis, D., 2011. Intelligent multi-sensor system for the detection and treatment of fungal diseases in arable crops. Biosyst. Eng. 108, 311–321.

Naidu, R.A., Perry, E.M., Pierce, F.J., Mekuria, T., 2009. The potential of spectral reflectance technique for the detection of Grapevine leafroll-associated virus-3 in two red-berried wine grape cultivars. Comput. Electron. Agric. 66, 38–45.

Oberti, R., 2003. Optical systems for assessing the healthy status of plants (in Italian). I Georgofili – Atti dell'Accademia dei Georgofili 50, 299–318.

Poutaraud, A., Latouche, G., Martins, S., Meyer, S., Merdinoglu, D., Cerovic, Z.G., 2007. Fast and local assessment of stilbene content in grapevine leaf by in vivo fluorometry. J. Agric. Food Chem. 55, 4913–4920.

Rumpf, T., Mahlein, A.-K., Steiner, U., Oerke, E.-C., Dehne, H.-W., Plümer, L., 2010. Early detection and classification of plant diseases with support vector machines based on hyperspectral reflectance. Comput. Electron. Agric. 74, 91–99.

Sankaran, S., Mishra, A., Ehsani, R., Davis, C., 2010. A review of advanced techniques for detecting plant diseases. Comput. Electron. Agric. 72, 1–13.

Stummer, B.L., Francis, L., Markides, A.J., Scott, E.S., 2003. The effect of powdery mildew infection on grape berries and wine composition and sensory properties of Chardonnay wines. Aust. J. Grape Wine Res. 9, 28–39.

West, J.S., Bravo, C., Oberti, R., Lemaire, D., Moshou, D., McCartney, H.A., 2003. The potential of optical canopy measurement for targeted control of field crop diseases. Annu. Rev. Phytopathol. 41, 593–614.

Yuan, L., Zhang, J.-C., Wang, K., Loraamm, R., Huang, W.-J., Wang, J.-H., Zhao, J.-L., 2013. Analysis of spectral difference between the foreside and backside of leaves in yellow rust disease detection for winter wheat. Precision Agric. 14, 495–511.

Zhang, J.-C., Pu, R.-L., Wang, J.-H., Huang, W.-J., Yuan, L., Luo, J.-H., 2012. Detecting powdery mildew of winter wheat using leaf level hyperspectral measurements. Comput. Electron. Agric. 85, 13–23.